Journal of Applied Electrochemistry 29: 685–692, 1999.

An investigation into the electrodeposition of Au–Cu-matrix particulate composites

B. BOZZINI[1], G. GIOVANNELLI[2] and P.L. CAVALLOTTI[2]
[1]*INFM – Facoltà di Ingegneria, Università di Lecce v. Arnesano, I-73100 Lecce, Italy;*
[2]*Dipartimento di Chimica Fisica Applicata, Politecnico di Milano v. Mancinelli 7, I-20131 Milan, Italy*

Received 12 January 1998; accepted in revised form 11 November 1998

Key words: alloys, composites, electrodeposition, gold–copper alloy

Abstract

The electrodeposition of AuCu/B_4C composites from alkaline baths containing free cyanide is described. The electrochemical behaviour of the bath and the metallographic and crystalline structures of the electrodeposited alloys were studied with and without addition of particles. Electrochemical instabilities were observed and their bearing on the structure of both pure matrix and composite electrodeposits is shown and elucidated. The electrochemical and structural conclusions on the AuCu/B_4C system are thought to be general for alloy-matrix composite plating with nonconductive particles.

1. Introduction

Work on the electrodeposition of composites in our group has achieved the definition of a quantitative metallographic procedure for the study of 3D particle distribution in metal matrix codeposits [1] and the elucidation and modelling of the phenomenon of preferential codeposition. The distribution of embedded particle diameters is different from that of the dispersed particles present in the bath [2].

As far as Au-matrix particulate ceramic composite deposition is concerned, high volume fractions ($C_F \simeq 30\%$) of embedded micrometric ceramic particles were obtained from acid citrate and phosphate baths with low (1–2%) B_4C loads; operating conditions and results are reported elsewhere [3]. Successful codepositions could not be carried out ($C_F < 2\%$) with polycrystalline diamond, α-Al_2O_3, γ-Al_2O_3 and SiC (mainly carborundum II with slight amounts of carborundum I and III, hence referred to simply as SiC) [4].

The scope of the present work is to present research on the possibility of obtaining Au-alloy-matrix electrodeposited composites: in this case Au–Cu matrices are considered. Preliminary experience with other precious metal and alloy systems includes the study of cyano-alkaline unalloyed Ag baths [4], with polycrystalline diamond, α-Al_2O_3, γ-Al_2O_3, SiC and B_4C dispersions. None of the above-mentioned ceramic powders allowed coverage factors in excess of 1%. Sizeable amounts of B_4C particles could be embedded only under dendritic growth at limiting current density conditions.

Cyano-alkaline Au–Ag baths of composition Au:Ag = 10:1 (wt %) and total metal content 10 g dm^{-3} with B_4C dispersion show unsatisfactory ceramic embedding. High volume-fraction codeposition of ceramic particles (C_F = 20–30%) in unalloyed Cu matrices (cyano-alcaline and neutral pyrophosphate baths) could be achieved only with B_4C; the rest of the above-mentioned ceramics did not give rise to codeposits with $C_F > 2\%$.

Study of the Au–Cu/B_4C system, with baths described elsewhere [5], allowed high C_F values to be achieved, but the cross sections of the deposits were characterised by marked compositional heterogeneities, brought about by the presence of the particles. This unusual phenomenology suggested a detailed study of the electrochemical processes involved in Au–Cu alloy and Au–Cu matrix composite deposition.

2. Experimental details

2.1. *Analytical methods*

Microscopic and structural work was carried out using SEM and XRD. Quantitative image analysis was performed as described in [1].

Electrochemical investigations on baths not containing particles were performed with the following equipment: potentiodynamic and galvanodynamic measurements carried out with a computer-controlled galvanostat–potentiostat, a Ag/AgCl RE was connected to the cathodic surface via a Piontelli lateral channel probe [6]. All the experiments were run in prismatic Pyrex cells with plane-parallel electrodes and magnetic stirring. Hydrodynamic conditions and current distribution were characterised [7]. Stirring velocity was set in order to obtain a Reynolds number of 10400.

The cathodic material was polycrystalline copper in the form of slabs. The cathodes were finished with a metallographic polish and were activated with sulphamic acid immediately before electrodeposition. The cathodically active surface, of area 6.25 cm^2, was defined with square PTFE windows. The anode was an expanded platinized titanium electrode. Galvanostatic and potentiodynamic measurements on baths with and without dispersion of ceramic particles were carried out in the pilot plant described in Section 2.2.

All the cathodic potentiodynamic experiments were run by scanning the cathodic potential from the immersion potential at a rate of 1 mV s^{-1}, the hysteretic behaviour of the cathodic kinetics was confirmed by replicated runs and with inverted potentiodynamic scans. Cathodic galvanodynamic measurements were performed with a scanning rate of 1 mA cm^{-2} s^{-1}.

As far as electrochemical measurements on the pilot plant are concerned, the measured cell potentials were corrected for ohmic drop and anodic overvoltage with suitable calibrations.

2.2. *Materials and methods*

The investigated Au–Cu electrodeposition bath was an alkaline cyanide bath whose composition and operating conditions are reported in Table 1.

Table 1. Composition and operating conditions for the cyanide Au–Cu bath

Composition	Operating conditions
Au^+ (as $KAu(CN)_2$)	5 g dm^{-3}
Cu^+ (as $K_2Cu(CN)_3$)	25 g dm^{-3}
Free KCN	15 g dm^{-3}
T	80 °C
pH	12
c.d.	3–12 mA cm^{-2}
Cell voltage*	−1.32 V
Deposition rate*	28–30 μm h^{-1}
Cathodic efficiency*	~90%

* Current density 7.5 mA cm^{-2} with B_4C (2 wt %)

Cyanoalkaline baths are reported to display a regular codeposition behaviour [8, 9], Au being the more readily deposited metal and Cu being deposited after the limiting current density (c.d.) for Au is attained. The morphology of the deposits is reported to be laminar and columnar [5, 10]. The potentiodynamic behaviour as a function of pH was studied in [5]; from the potentiodynamic curve reported it is possible to observe one limiting c.d., which can be assigned to Au^+ reduction, and a monotonic growth of c.d. against potential, at variance with the sigmoidal behaviour observed in the present work (Section 3.1). The potentiodynamic curves reported in [5] show that Cu/Cu^+ equilibrium potential grows nobler as pH decreases (pH actually controls the amount of free CN^- present in the bath). The ceramic material was B_4C and the particles had an average diameter of 2.52 μm; the bath loading was 20 g dm^{-3} (~2% by weight).

The electrochemical reactor (Figure 1) was a Pyrex cylinder (ϕ = 140 mm, h = 100 mm) containing 1 dm^3 of solution, temperature control within $\pm$0.5 °C was achieved with a thermostatic bath. The inner and outer concentric cylindrical anodes were two platinised Ti expanded mesh electrodes with ϕ = 140 and 40 mm, respectively, and h = 40 mm; the outer anode was fixed to the Pyrex wall of the reactor and the inner one to the central shaft. The cathodes were metallographically polished polycrystalline copper cylinders, the cathodes were activated with sulphamic acid before deposition.

Revolution of the cathode (cathode revolution radius 45 cm) was obtained using a special crank device described elsewere [11]. Rotation of the shaft

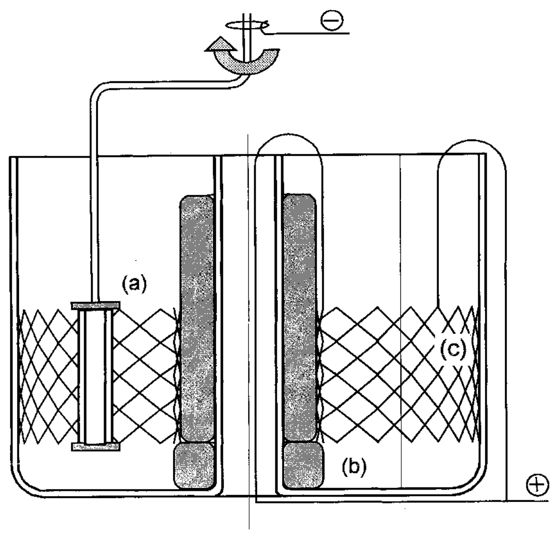

Fig. 1. Electrochemical codeposition reactor with cathode revolution: (a) revolving cathode; (b) internal anode; (c) peripheral anode.

(120 rpm) was controlled using a stepping motor and electrical connection was provided with a sliding contact. Under these conditions a Reynolds number of 5655 was obtained, corresponding to turbulent flow [12].

3. Experimental results and discussion

3.1. *Electrochemical measurements*

Electrochemical measurements were carried out by controlling the cathodic potential, c.d. and cell potential. Potentiodynamic scans measured with a scanning rate of 1 mV s^{-1}, gave a sigmoidal current–voltage plot (Figure 2), similar to that for electrodic systems displaying passivation phenomena. By scanning the c.d. (galvanodynamic measurement) in the forwards and backwards directions it was possible to observe a hysteretic behaviour (Figure 3) consistent with the sigmoidal potentiodynamic behaviour (Figure 2). Both potentiodynamic and galvanodynamic measurements were extremely reproducible, as seen in the overlap of the plots corresponding to replicate runs.

3.2. *Electrodeposition experiments*

Very low Au contents were obtained from the bath at $T < 60$ °C and very low volume fractions of particles were embedded at $T > 85$ °C. Samples prepared in the reactor described in Section 2.2 by applying a c.d. in the range 4–12 mA cm^{-2} under cell potential control, corresponding to cathodic overvoltages in the range from (−0.4) to (−1.2) V (Ag/AgCl), tended to show a banded

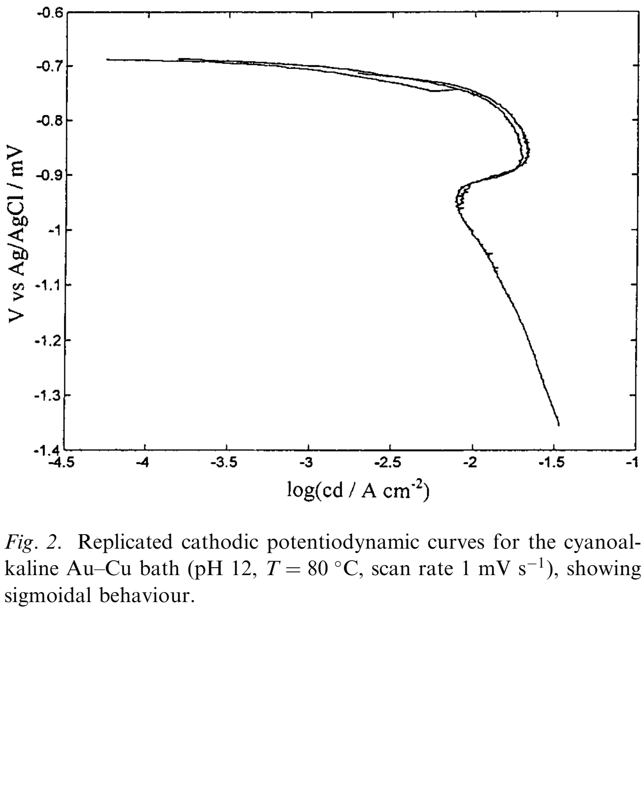

Fig. 2. Replicated cathodic potentiodynamic curves for the cyanoalkaline Au–Cu bath (pH 12, $T = 80$ °C, scan rate 1 mV s^{-1}), showing sigmoidal behaviour.

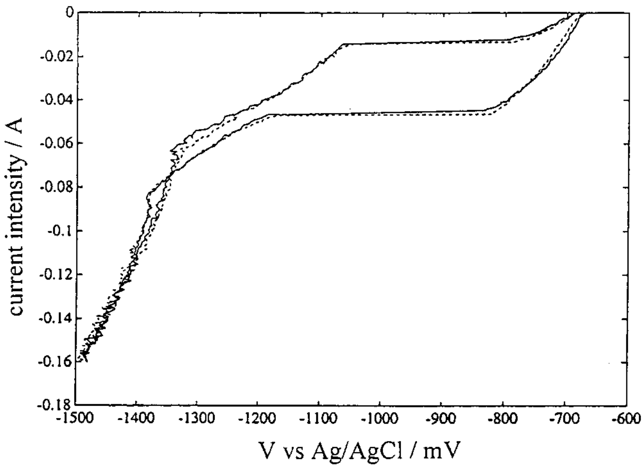

Fig. 3. Replicated cathodic galvanodynamic curves for the cyanoalkaline Au–Cu bath (pH 12, $T = 80$ °C, scan rate 1 mA cm^{-2} s^{-1}), showing sigmoidal behaviour (cathode area 4 cm^2).

structure (Figure 4). The sequence of bands was analysed by EDS in the line-scanning mode and showed an alternation of Au-enriched and Au-depleted layers.

The preparation of samples under c.d. control, starting form c.d. near zero, and subsequently increasing the c.d. in steps of 1 mA min^{-1}, made it possible to reach c.d.s of approximately 10 mA cm^{-2} without exceeding the critical cathodic potential value of −0.8 V (Ag/AgCl). Such deposition conditions, characterised by voltages lower than −0.8 V (Ag/AgCl), were stable for times in excess of 1 h; Au-yellow deposits with a uniform morphology (no banded structure) and a constant composition (98–90% Au, for c.d.s decreasing in the range 4–10 mA cm^{-2}) were obtained.

It was also possible to obtain similar results under cell potential control, provided a suitable margin of safety

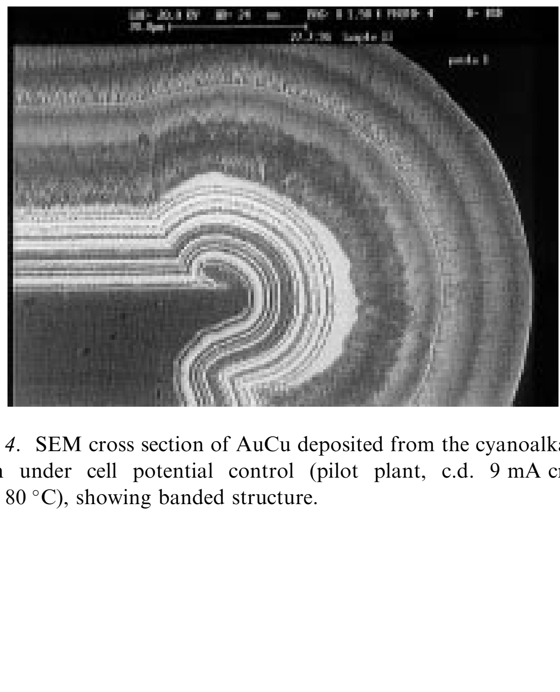

Fig. 4. SEM cross section of AuCu deposited from the cyanoalkaline bath under cell potential control (pilot plant, c.d. 9 mA cm^{-2}, $T = 80$ °C), showing banded structure.

was adopted in order to avoid instabilities due to uncontrollable cell resistance variations (variations of hydrodynamic conditions and of temperature, see Section 3.4).

If the c.d. was increased (under c.d. control) beyond 10–11 mA cm^{-2}, the cell potential suddenly jumped by -1.25 V; this potential jump corresponds to transition to the second branch of the hysteresis curve. Similarly to the first branch, it was possible to operate the bath in the second branch with c.d.s varying continuously in the range 4–12 mA cm^{-2} and cathodic voltages from -1.10 to -1.35 V (Ag/AgCl) and provided the c.d. was not lowered below 4–5 mA cm^{-2}, corresponding to cathodic potentials of -1.1 V (Ag/AgCl). Under these conditions homogeneous deep pink deposits were obtained with Au contents varying continuously in the range 40–56%. The c.d.–composition relation is shown in Figure 5.

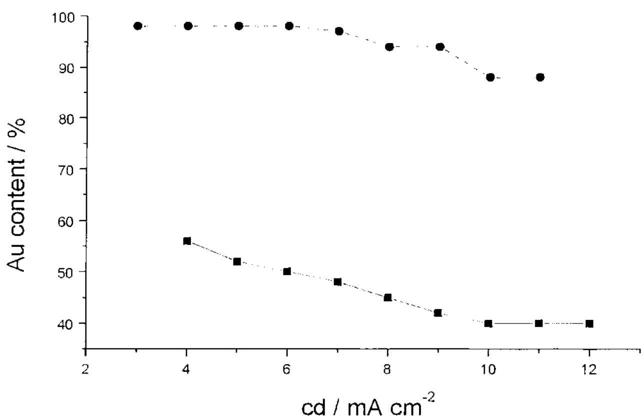

Fig. 5. Au contents in deposits obtained from the cyanoalkaline bath in the high-Au (●) and low-Au (■) branches of the c.d. against potential curve.

3.3. *X-ray diffractographic studies*

Typical X-ray diffractograms of coatings obtained in the two branches of the hysteresis loop with the same c.d. ddc (9 mA cm^{-2}) (Figure 6) showed the formation of solid solutions and the absence of 'mixed crystals', in accordance with [13], but at variance with [5]; Végard's law, as applied to the Au–Cu system [14], gave data consistent with EDS results. Crystallite dimensions D (as evaluated by the Scherrer method) were much smaller in the high-Cu branch: high-Au branch $D = 66.7$ nm, high-Cu branch $D = 12.4$ nm.

3.4. *Discussion of the hysteresis loop*

The sigmoidal behaviour observed in the potentiodynamic measurements, and the corresponding hysteresis in the galvanodynamic curves, can be justified as follows. Only one electroactive species exists for Au^+ [15] and the build-up of CN^- following cathodic deposition does not show cathodic inhibiting effects, as observed from the constancy of the Tafel slope in the potentiodynamic curves from baths containing only Au^+ cyanide complexes. In contrast, as far as Cu^+ is concerned, three different cyano-complexes are known; the activity of the Cu^+ cation is correspondingly changed and, consequently, the equilibrium potentials of the Cu^+/Cu couple vary and tend to become less noble as the CN^-/Cu^+ ratio increases [16, Figure 2]. Finally, an approximately asymptotic value is reached at about -0.8 mV(Ag/AgCl).

At low c.d.s the action of CN^-, released at the cathode owing to Au^+ discharge, tends to inhibit Cu deposition through the stabilization of Cu cyanocom-

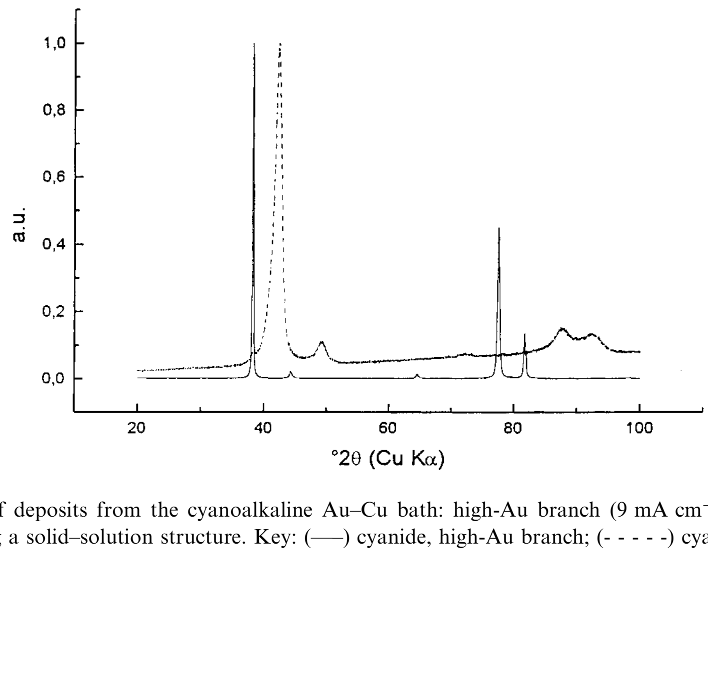

Fig. 6. X-ray diffractograms of deposits from the cyanoalkaline Au–Cu bath: high-Au branch (9 mA cm^{-2}, Au 98%) and low-Au branch (9 mA cm^{-2}, Au 42%) showing a solid–solution structure. Key: (—–) cyanide, high-Au branch; (- - - - -) cyanide, low-Au branch.

plexes with higher coordination numbers and progressively less noble potentials.

At the lowest c.d.s, the limited surface concentration of CN^- released by the Au^+ complex, stabilises the electroactive Cu^+ cyanocomplexes with a low coordination number. As the c.d. increases, the increase in CN^- released at the surface leads to the formation of cyanocomplexes with high coordination number, which are not electroactive at the current potential; such species are most probably adsorbed at the cathode [17] and tend to reduce the amount of active cathodic surface, thus leading to lower c.d. values at the same electrode potential. The electroactivity threshold for the adsorbed high-cyanocomplexes is finally reached due to further increases in electrode potential, the c.d. consequently recommences growth as the cathodic potential increases. This simple model is confirmed by potentiodynamic runs performed at different scan rates: high scan rates (typically 10 mV s^{-1}), related to lower amounts of released CN^-, tend to suppress the sigmoidal behaviour, while slow scans (typically 0.1 mV s^{-1}), implying a high amount of CN^- released per unit voltage increase, bring about an enhancement of this feature.

Further experimental evidence supports this explanation:

(i) The phenomenon does not depend on the composition of the cathode, since the hysteresis can also be observed for temperatures in excess of 80 °C, in which case the compositon of the alloy deposited at the critical c.d. is richer in Au. Further, XRD studies do not show any structural differences among deposits obtained on both branches of the hysteresis loop. Crystallite dimensions for the high-c.d. branch are smaller, as observed above (Section 3.3). This result agrees with the hypothesis of electrocrystallization under cathodic inhibition conditions [18].

(ii) The phenomenon seems to be connected neither with hydrogen evolution, as the cathodic current efficiency is practically unchanged in the whole of the studied c.d. range, nor with changes to the bath, as it is observed with high reproducibility with both fresh and aged baths.

(iii) The phenomenon is observed only when alloy is being deposited, as mentioned above. Single-metal baths do not display such a sigmoidal behaviour. In addition, the phenomenon seems to be related to the amount of free CN^- present in the bath, since the formation of banded structures can also be observed when free cyanide forms in baths initially containing only complexed cyanide, owing to prolonged operation [19]; electrochemical measurements carried out at pH 7 (conditions under which the free-cyanide concentration is severely reduced) show a marked decrease of the sigmoidal behaviour of potentiodynamic curves.

(iv) Resolution of the alloy c.d. against potential curves into partial current densities for gold and copper [8], reveal that the gold partial current density acquires a negative slope in the high current density region.

(v) Potentiodynamic measurements performed on the same bath without any $KAu(CN)_2$ (Figure 7) show

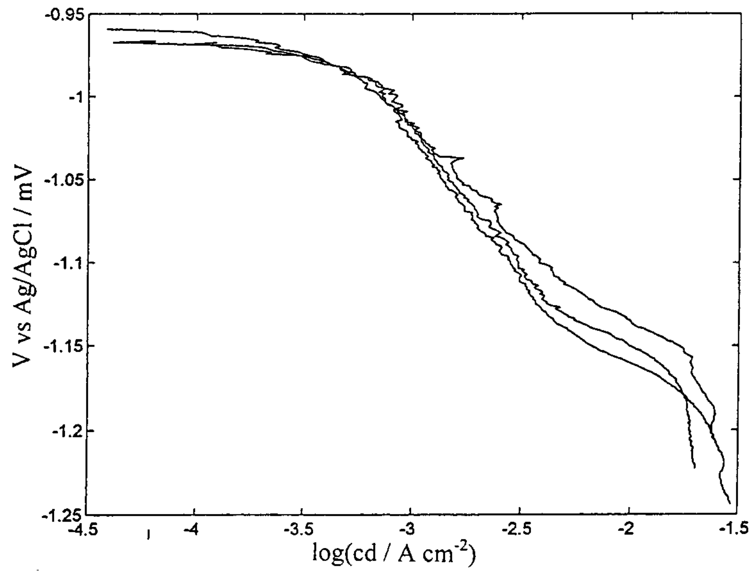

Fig. 7. Replicated cathodic potentiodynamic curves for the cyanoalkaline Cu bath (pH 12, $T = 80$ °C, scan rate 1 mA cm^{-2} s^{-1}), showing two Tafel slopes.

Table 2. Cathodic voltages are reported for electrodeposition with and without B_4C in the high-Cu and high-Au branches of the hysteresis loop

i/mA cm^{-2}	V (Ag/AgCl) low-i branch no B_4C	V (Ag/AgCl) low-i branch B_4C 2%	V (Ag/AgCl) high-i branch no B_4C	V (Ag/AgCl) high-i branch B_4C 2%
0	−0.36	−0.37		
2	−0.57	−0.56		
4	−0.65	−0.65	−1.1	−1.1
6	−0.75	−0.72	−1.13	−1.13
8	−0.77	−0.75	−1.2	−1.18
10	−0.8	−0.78	−1.25	−1.23
12			−1.32	−1.30
14			−1.55	−1.55

the presence of two mechanisms for the discharge of Cu cyanocomplexes, which can be identified with two different Tafel slopes ($B_1 = 164.3 \pm 14.6$ mV dec^{-1}, $B_2 = 54.23 \pm 8.01$ mV dec^{-1}) and a transition potential $E_{1\to 2} = -1138.7 \pm 23.7$ mV (Ag/AgCl), corresponding to $Cu(CN)_4^{3-}$ becoming the majority species [16].

The sigmoidal behaviour of the potentiodynamic curve observed in Figure 2 brings about dynamic instabilities of the cathodic system. In the case of an ideal potentiostatic experiment the characteristic curve of the generator can be expressed as $\partial i/\partial\eta = \infty$; in this case the intersection of the cathodic characteristic curve and that of the generator is single valued: the dynamics of the working point is therefore stable.

In the case of an ideal galvanostatic experiment (the actual galvanostatic experiment is a good approximation of the ideal one) the characteristic curve of the generator can be expressed as $\partial i/\partial\eta = 0$; in this case there exists a critical c.d. interval in which the intersection of the cathodic characteristic with that of the generator is triple valued. The working point for intermediate potentials is thus unstable, whilst working points corresponding to potentials lower and higher than the critical interval limits are stable. It follows that the working point can jump form the high-Cu to the high-Au branch, as shown in Figure 3.

In the case of an experiment with a real potentiostat–galvanostat, where the generator supplies a voltage U and the cell is connected to the generator with lines having a finite resistance R. It follows that $V = U + \eta_{\text{ref}} - \eta_{\text{cell}} = Ri(\eta)A$, where η_{ref} is the electrode voltage, η_{cell} is the cell voltage, A is the electrodically active surface area and $i(\eta)$ is the potentiodynamic curve. The stability condition in this case is $-\mathrm{d}i(\eta)/\mathrm{d}\eta < \frac{1}{R}$. The stability of the electrodic system thus depends on the values of 'stray' resistances (including electrolyte resistance) and on the effective electrode area in the case of potentiodynamic curves with a negative resistance; this kind of dynamic behaviour explains why laminar deposits are obtained in the pilot plant.

3.5. *Electrochemical behaviour in the presence of nonconductive particles*

The addition of particles to the bath brings about only limited variations of the potentiodynamic curve and of the cathodic efficiency. Table 2 shows cathodic voltages, corresponding to electrodeposition with and without particles in the two branches of the hysteresis loop.

Figure 8 shows a SEM metallographic cross section of an electrodeposit obtained in the high-Cu branch of the hysteresis loop at a c.d. of 5 mA cm^{-2}. Compositional heterogeneities can be observed (backscattered electron imaging), the average composition of the coating being 40% Au. The Au content for a coating obtained under the same operating conditions without particle addition is 52% . Figure 9 shows a metallographic cross section for a layer obtained by depositing in the high-Au branch of the hysteresis loop at a c.d. of 9.5 mA cm^{-2} with a cathodic voltage of −0.8 V Ag/AgCl; the inner layer, which was obtained before adding particles to the bath, has a Au content of 90%, the external one, a B_4C-containing codeposit, shows compositional heterogeneities whose nature is clearly different from the previous

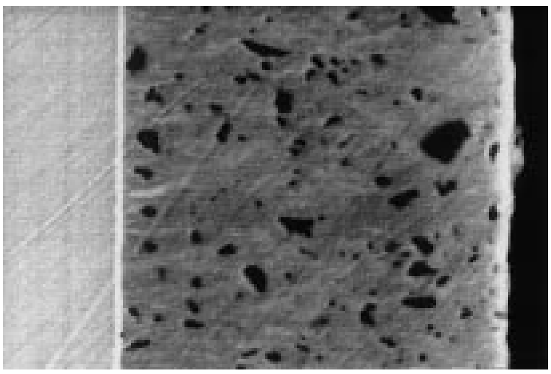

Fig. 8. SEM cross section of $AuCu/B_4C$ deposited from the cyano-alkaline bath in the high-Cu branch of the hystersis loop (pilot plant, Au 40%, c.d. 5 mA cm^{-2}, $T = 80$ °C), showing 'crests' with a higher Au content (deposition direction: from left to right, backscattered electrons, compositional contrast).

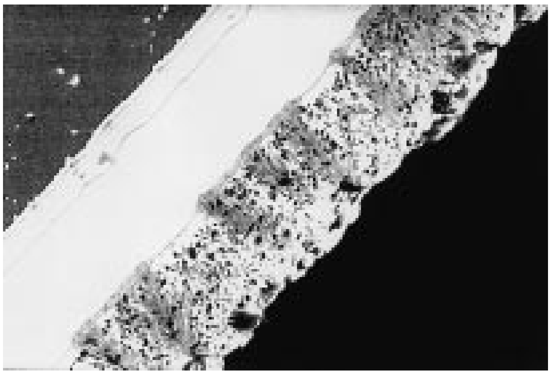

Fig. 9. SEM cross section of AuCu/B_4C deposited from the cyano-alkaline bath in the high-Au branch of the hystersis loop (pilot plant, c.d. 9.5 mA cm^{-2}, $T = 80$ °C, pure matrix layer: Au 90%, average Au content of composite layer 42%, clear glass 70%, dark areas 14%).

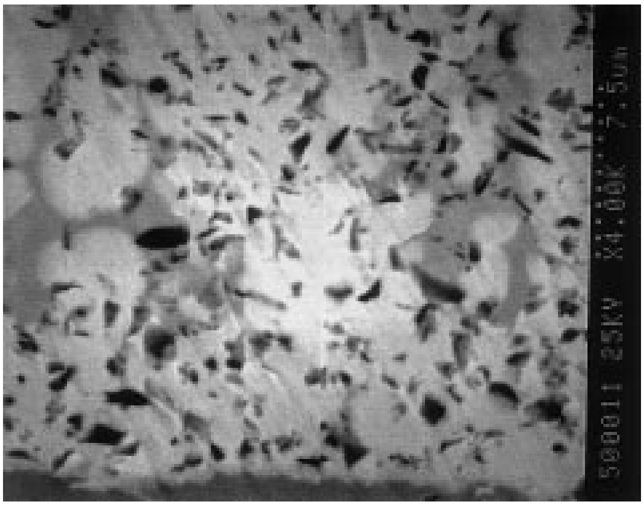

Fig. 11. SEM cross section of AuCu/B_4C deposited from the cyano-alkaline bath in the high-Au branch of the hystersis loop (pilot plant, c.d. 4 mA cm^{-2}, $T = 80$ °C), showing 'tails' with a higher Cu content (deposition direction: upwards, backscattered electrons, compositional contrast, c.d. 5 mA cm^{-2}, Au 76%), showing a solid–solution structure.

one (SEM backscattered electrons image clear areas 70% Au, dark ones 14% Au, average composition for the whole section 42%). Similar morphologies can be observed for deposits obtained at any point of the high-Au branch of the hysteresis loop (Figure 10).

The increase in the average content of the less noble metal in the electrodeposited alloy, which can be observed in both branches of the hystersis loop, can be explained on the basis of the increase in the average cathodic c.d. due to the presence of nonconductive particles.

A closer look at the micrographs corresponding to the high-Cu branch (Figure 8, backscattered electron SEM image) shows the presence of alloy 'crests' with a higher Au content (the nobler metal under the prevailing deposition conditions) in the material deposited immediately before particle embedding. Similarly, a closer look at the micrographs corresponding to the high-Au branch (Figure 11) shows the presence of alloy 'tails' with a higher Cu content (the less noble metal under the prevailing deposition conditions) in the material deposited immediately after particle embedding.

The presence of 'crests' can be explained in terms of a local decrease of c.d. due to cathodic screening by each nonconductive particle approaching the cathodic surface until contact is achieved. In the presence of the above discussed hysteretic phenomena, backscattered electron images show high and low local c.d. areas through compositional contrast. The presence of 'tails' can be explained in terms of a local c.d. increase, due to cathodic screening brought about by each non-conductive particle being incorporated. Similarly, in the presence of the hysteresis, backscattered electron images show high local c.d. areas through compositional contrast.

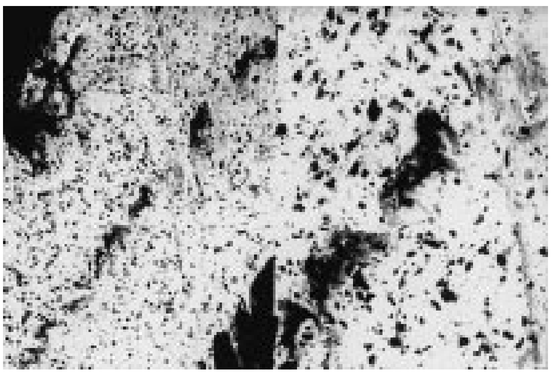

Fig. 10. SEM cross section of AuCu/B_4C deposited from the cyano-alkaline bath in the high-Au branch of the hystersis loop (pilot plant, c.d. 5 mA cm^{-2}, $T = 80$ °C).

4. Conclusions

(i) High free-cyanide cyanoalkaline baths display a sigmoidal potentiodynamic behaviour and, correspondingly, a hysteretic galvanodynamic behaviour. Metallographic cross sections of deposits obtained from such baths under cell potential control show a laminar structure. This behaviour can be explained in terms of the absorption of cuprous complexes with a high CN^- coordination number, which are not electroactive for low cathodic overvoltage values.

(ii) Embedding of nonconductive particles in all the investigated baths for alloy deposition correlates with an increase in the content of the less noble

alloying element. This phenomenon can be interpreted in terms of an increase in the average deposition c.d. due to cathodic screening effects brought about by the presence of the insulating particles: (a) In the high-c.d. branch, memory of local c.d. decreases is frozen into the formation of areas enriched in the nobler metal in the 'sticking' zones of nonconductive particles; (b) In the low-c.d. branch, memory of local c.d. increases due to the point effect, is frozen into the formation of areas enriched in the less noble metal in the zones behind the embedded particles.

Contributions of the authors

B.B. and G.G. jointly planned and carried out the experimental and modelling work, P.L.C. supervised the research and revised the manuscript.

References

1. B. Bozzini, P.L. Cavallotti, G. Giovannelli, B. Brevaglieri and S. Natali, *Praktische Metallographie – Practical Metallography* **33** (1996) 130.
2. B. Bozzini, G. Giovannelli and P.L. Cavallotti, *J. Microsc.* **185** (1997) 283.
3. G. Bollini, B. Bozzini, G. Giovannelli and P.L. Cavallotti, *AIFM. Galvanotecnica e Nuove Finiture* **6** (1996) 22.
4. B. Bozzini, P.L. Cavallotti and G. Giovannelli, *Proc. Royal Microsc. Soc.* **31** (1996) I, 41.
5. E. Raub and F. Sautter, *Metalloberfläche* **10** (1956) 65.
6. R. Piontelli. *Corrosion* **9** (1953) 115.
7. B. Bozzini, F. Pavan, G. Bollini and P.L. Cavallotti, *Trans. IMF* **75**(5) (1997) 175.
8. A. Brenner, 'Electrodeposition of Alloys' (Academic Press, New York, 1963).
9. E. Raub and K. Müller, 'Fundamentals of Metal Deposition' (Elsevier, Amsterdam, 1967), pp. 96–7.
10. H.J. Wiesner and W.B. Distler, *Plating* **56** (1969) 799.
11. B. Bozzini, G. Giovannelli and P.L. Cavallotti, 'Hydrodynamic effects in the electrodeposition of composites'. Submitted for ISE '99.
12. V.G. Levich, 'Physicochemical Hydrodynamics' (Prentice Hall, Englewood Cliffs, NJ, 1962), p. 34.
13. R. Rochat, *Bull. Ann. Soc. Suisse de Chronometrie* **4** (1957) 45.
14. A. Guinier. 'Théorie et Technique de la Radiocristallographie' (Dunod, Paris, 1956), p. 372.
15. W.S. Rapson and T. Groenewald, '*Gold Usage*' (Academic Press, London, 1978), p. 214.
16. A. Katagiri, H. Inoue and N. Ogure. *J. Appl. Electrochem.* **27** (1997) 529.
17. H. Fischer. 'Elektrolytische Abscheidung und Elektrokristallisation von Metallen' (Springer Verlag, Berlin, 1954), p. 618.
18. R. Winand, *Hydrometallurgy* **29** (1992) 567.
19. H.J. Wiesner and W.P. Frey, *Plating* **56** (1969) 527.
20. R. Cathrein and M. Denemark. *US Patent 3 380 814* (1968).
21. B. Bozzini, G. Giovannelli, M. Ratti and P.L. Cavallotti, submitted to *J. Electrochem. Soc.* (accepted for publication).